COMMUNICATION

Check for updates

Integrated cascade catalysis of microalgal bioenzyme and inorganic nanozyme for anti-inflammation therapy†

Qi-Wen Chen,‡ Meng-Wei Cao,‡ Ji-Yan Qiao, Qian-Ru Li and Xian-Zheng Zhang [ID]*

Combinations of multiple enzymes for cascade catalysis have been widely applied in biomedicine, but the integration of a natural bioenzyme with an inorganic nanozyme is less developed. Inspired by the abundant content of superoxide dismutase (SOD) in *Spirulina platensis* (SP), we establish an integrated cascade catalysis for anti-inflammation therapy by decorating catalase (CAT)-biomimetic ceria nanoparticles (CeO$_2$) onto the SP surface *via* electrostatic interaction to build microalgae-based biohybrids. The biohybrids exhibit combined catalytical competence for preferentially transforming superoxide anion radicals (O$_2^{\bullet-}$) to hydrogen peroxide (H$_2$O$_2$), and subsequently catalyzing H$_2$O$_2$ disproportionation to water and oxygen. In ulcerative colitis and Crohn's disease, the biohybrids reveal a satisfactory therapeutic effect owing to the synergistic reactive oxygen species (ROS)-scavenging capacity, suggesting a new train of thought for enzyme-based biomedical application.

New concepts

The combination of multiple enzymes for cascade catalysis has been widely explored in biomedical applications, but the integration of microbial bioenzymes with inorganic nanozymes is less developed in this field. In this study, a biotic/abiotic biohybrid system that combines a microalgal bioenzyme with an inorganic nanoenzyme is established for anti-inflammation therapy through executing a cascade catalysis to eliminate O$_2^{\bullet-}$ and H$_2$O$_2$. In mouse models of ulcerative colitis (UC) and Crohn's disease (CD), the fabricated biohybrid exhibits a satisfactory therapeutic effect and effectively protected colonic damage. Hence, the biohybrid formulation shows an excellent therapeutic effect for inflammatory bowel disease and suggests an innovative idea for fabricating multiple enzyme-based cascade catalysis.

1. Introduction

Due to their diverse catalytical activities that are suitable for disease intervention, natural bioenzymes or inorganic nanozymes have been widely exploited for biomedical applications.[1–3] Nevertheless, the therapeutic ability of the particular enzyme is usually restricted by its single catalytical property, which could be inapplicable in complex pathological settings because of the incomplete catalytic results.[4] In order to solve the single catalytical defect of a specific enzyme, combining multiple enzymes for cascade catalysis has been developed by employing bioenzymes or nanozymes.[3,5–12] Among the developed combined configurations

Key Laboratory of Biomedical Polymers of Ministry of Education & Department of Chemistry, Wuhan University, Wuhan, 430072, P. R. China.
E-mail: xz-zhang@whu.edu.cn

† Electronic supplementary information (ESI) available. See DOI: **https://doi.org/10.1039/d2nh00572g**

‡ The two authors contributed equally to this paper.

of various enzymes, the combination of natural bioenzymes with inorganic nanozymes has been less explored.[13] Additionally, the choice of enzyme-carrying cargoes that efficiently load enzymes and protect their bioactivity is also an important challenge.[14,15]

In particular, some microorganisms show special bioactivity and express a high content of special bioenzymes.[16] The abundant chemical groups on and large area of the microbial cell surface also provide ideal attachment points for further modification and protection.[17,18] These merits endow microorganisms with an ideal platform for cascade catalysis by combing heterogeneous enzymes.[19] As a food-grade probiotic microalga, *Spirulina platensis* (SP) exhibits a potent prevention effect in gastrointestinal tract diseases relying on its special bioactivity and therapeutic protein enzymes, or serving as a versatile carrier owing to the helical shape that supports modification and prolonged retention in the gut.[20,21] Also, the therapeutic protein enzymes within SP could be protected from inactivation by the intact microbial cell structure when passing through digestive juices in the gastrointestinal tract.[22–25] The high content of superoxide dismutase (SOD) expressed by SP may mainly transform toxic superoxide anion

radicals ($O_2^{\bullet-}$) to hydrogen peroxide (H_2O_2), thus endowing it with potential therapeutic ability in inflammatory bowel disease (IBD).[26–28] But H_2O_2 is still a typical inflammatory molecule that mediates the pathogenesis of IBD. Therefore, the introduction of catalase (CAT) is necessary to integrate the natural SOD of SP for the cascaded disproportionation of toxic $O_2^{\bullet-}$ to nontoxic oxygen and water.

It has been reported that ceria nanoparticles (CeO_2) are biocompatible and possess highly effective CAT-biomimetic bioactivity.[29] Therefore, the cascade reaction was built by decorating the nanozyme of CeO_2 onto SP for thoroughly eliminating $O_2^{\bullet-}$ and H_2O_2 in IBD therapy. CeO_2 was first synthesized and modified by positively charged oligochitosan to convert the surface potential from a negative potential to a positive potential. Then, the positively charged CeO_2 nanozymes were loaded onto the surface of the SP biocarrier *via* electrostatic absorption. The fabricated biohybrids (designated SP@COS-CeO₂) can first catalyze $O_2^{\bullet-}$ to H_2O_2 with a natural SOD bioenzyme belonging to SP; then H_2O_2 is subsequently disproportionated into oxygen and water by the loaded CeO_2 nanozyme. The tandem reaction is expected to neutralize the inflammatory $O_2^{\bullet-}$ and H_2O_2 to cure IBD (Scheme 1). In mouse models of ulcerative colitis (UC) and Crohn's disease (CD), the fabricated biohybrids exhibited a satisfactory anti-inflammation effect and effectively prevented colonic damage. This study provides a new strategy for enzyme-based disease therapeutics by establishing cascade catalysis between a natural bioenzyme and an artificial nanozyme.
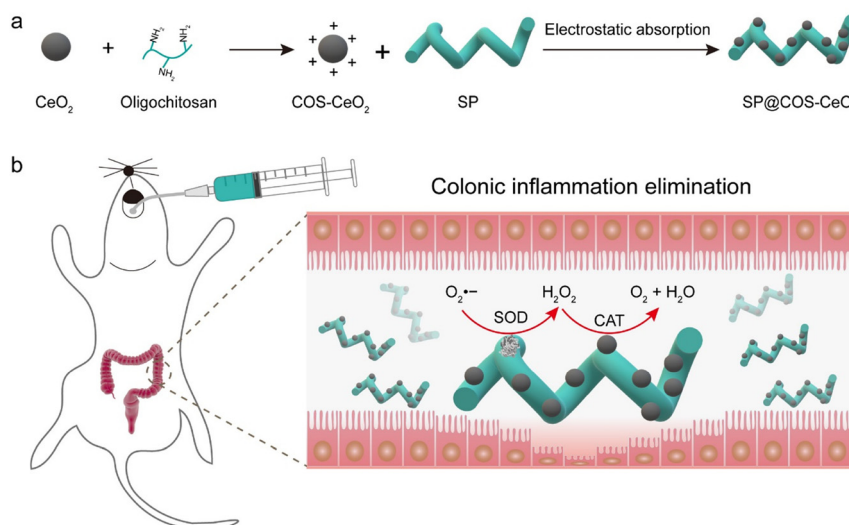
2. Results and discussion

2.1. Cultivation and characterization of SP

SP was cultivated in Zarrouk medium placed in an incubator with a photoperiod of 12 h light/12 h dark and a light intensity of 2000 lux, and harvested until the green SP filled a triangular glass bottle (Fig. 1a). For convenience of use, fresh SP was washed

and lyophilized (Fig. 1b). A scanning electron microscopy (SEM) image showed that the lyophilized SP has a standard helical shape, with a length of about 400–600 μm and a cell diameter of about 5–8 μm (Fig. 1e). Because of the presence of abundant chlorophyll, SP can emit strong red fluorescence under an appropriate excitation wavelength ($\sim$605 nm). The bright field and fluorescence images showed the helical morphology and fluorescence characteristics of SP (Fig. 1c and d). The SOD activity of SP was detected using a Total SOD Elisa Assay Kit with WST-8. As shown in Fig. 1f, SP exhibited an inhibition rate of about 68% against $O_2^{\bullet-}$, indicating that SP has high SOD bioactivity. We also investigated the stability of SP in simulated gastric juice (SGF). As shown in Fig. 1g, after SGF treatment, there was a negligible change in the shape and length of the SP cells. Meanwhile, the fluorescence feature of SP was not weakened, indicating that the chlorophyll structure had not been destroyed. These results demonstrated that SP has good tolerance to SGF, which promises applicability when serving as a biotherapeutics platform for gastrointestinal tract application.

2.2. Synthesis and characterization of CeO₂ and COS-CeO₂

To achieve cascade catalysis, CeO_2 nanocrystals were first synthesized by reacting cerium(III) nitrate with 6-aminohexanoic acid (AHA) *via* an aqueous phase synthesis method.[30] In order to conveniently decorate CeO_2 onto SP, chitosan oligosaccharides (COS) were modified on the surface of CeO_2 nanoparticles *via* electrostatic interaction to obtain COS-CeO₂. According to transmission electron microscopy (TEM) images, both CeO_2 and COS-CeO₂ nanoparticles have a small diameter with a well-structured crystal (Fig. 1h and Fig. S1, ESI†). The cubic fluorite structure of CeO_2 and COS-CeO₂ nanoparticles was confirmed by X-ray diffraction (XRD) patterns (Fig. 1i). After good preparation of the CeO_2 and COS-CeO₂, the CAT-like activity of the two nanoparticles was evaluated by monitoring the amount of oxygen produced by the catalytic decomposition of H_2O_2. As shown in Fig. 1j and k, both nanoparticles exhibited excellent CAT-like catalytic performance.

Scheme 1 Schematic illustration of (a) process of synthesizing SP@COS-CeO₂ and (b) anti-inflammation therapy in IBD *via* cascade catalysis.
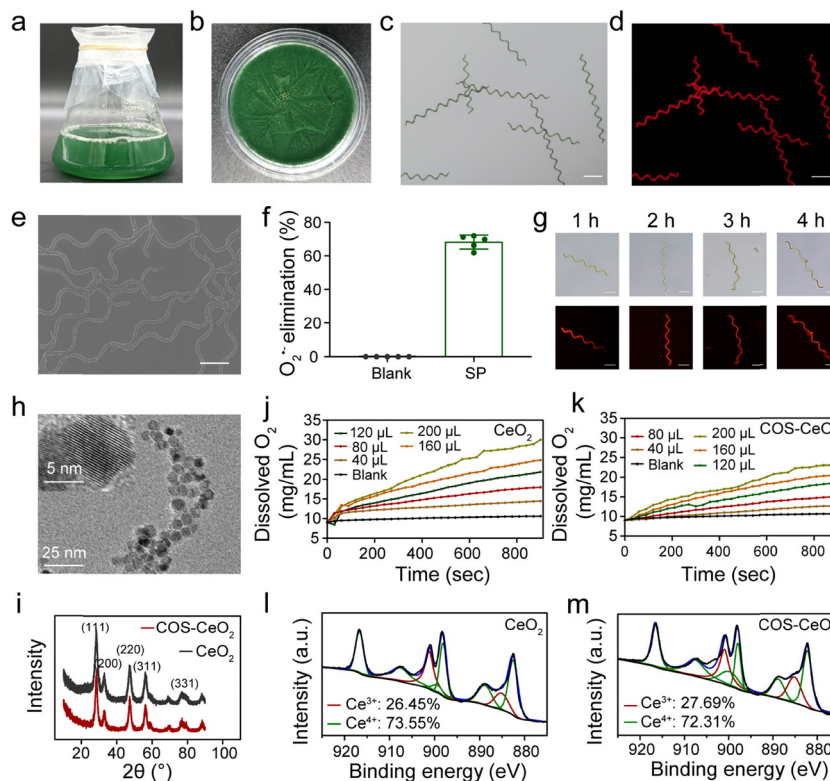
Fig. 1 Characterization of SP, CeO_2 and COS-CeO_2. (a) Fresh SP cultivated in Zarrouk medium and (b) its lyophilized powder. (c) Bright-field and (d) fluorescence images of SP. Scale bar = 100 μm. (e) SEM image of SP. Scale bar = 50 μm. (f) Percentage of superoxide radical elimination catalyzed by SP owing to its SOD activity. (g) The bright field and fluorescence images of SP after treatment with SGF (pH = 1.2; pepsin: 3.2 mg mL^{-1}) for 1, 2, 3 or 4 h, respectively. (h) TEM image of COS-CeO_2 (inset: high-resolution TEM image of COS-CeO_2). (i) XRD patterns of CeO_2 and COS-CeO_2. (j) Dissolved oxygen generated from the catalyzed decomposition of H_2O_2 by CeO_2 and (k) COS-CeO_2 (Ce: 2600 μg mL^{-1}). (l) Ce 3d XPS spectra of CeO_2 and (m) COS-CeO_2.

Compared with CeO_2, the CAT-like activity of COS-CeO_2 was slightly decreased, which could be ascribed to the shielding effect of COS. Since the enzyme-like catalytic performance of nanoscale CeO_2 depends on the ratio of Ce^{3+} and Ce^{4+} on the surface, we quantified the species of Ce valence by X-ray photoelectron spectra (XPS). As shown in Fig. 1l and m, the ratio of Ce^{3+}/Ce^{4+} in CeO_2 (Ce^{3+}: 27.69%; Ce^{4+}: 72.31%) was nearly equal to that of COS-CeO_2 (Ce^{3+}: 26.45%; Ce^{4+}: 73.55%), which indicated that the catalytic property of CeO_2 had not been affected by modification with COS. Additionally, the catalytic property of COS-CeO_2 was less weakened by SGF, as shown in Fig. S2 (ESI†), which also suggested that COS-CeO_2 is suitable for application in gastrointestinal tract catalysis.

2.3. Synthesis and characterization of SP@COS-CeO_2

The loading of CeO_2 nanoparticles onto SP was achieved by electrostatic interaction between positively charged COS-CeO_2 and negatively charged SP (Fig. S3, ESI†). SEM (Fig. 2a) and SEM-assisted element mapping (Fig. S4, ESI†) clearly demonstrated that CeO_2 was steadily attached onto the SP surface. As shown in Fig. 2c, the Fourier transform infrared (FTIR) spectrum of SP showed the characteristic absorption peaks of protein at 1650 cm^{-1} and 1537 cm^{-1}, corresponding to C=O bond stretching and N–H bond bending, respectively. The peak

at 1056 cm^{-1} in COS-CeO_2 spectrum is the absorption peak of CO_3^{2-}, because CO_2 in the air is easily absorbed by CeO_2. The above characteristic absorption peaks of both SP and COS-CeO_2 were observed in the FTIR spectrum of SP@COS-CeO_2, further confirming the successful loading of CeO_2 onto SP. To optimize the loading process of SP, different equivalents of COS-CeO_2 (corresponding to Ce contents of 650, 1300, 2600, 5200 and 11 400 μg mL^{-1}) were added to 10 mL of SP suspension (500 μg mL^{-1}) for reaction. Inductively coupled plasma-atomic emission spectrometry (ICP-AES) was used to detect the Ce content in SP@COS-CeO_2 to determine the load efficiency of SP. As shown in Fig. S5a (ESI†), the loading efficiency increased following enhancement with reaction equivalents of COS-CeO_2. Nevertheless, the structure of SP was severely damaged after adding 8 equivalents (Ce: 5200 μg mL^{-1}) or 16 equivalents (Ce: 11 400 μg mL^{-1}) of COS-CeO_2 (Fig. S5b, ESI†). Therefore, the optimal reaction equivalent of COS-CeO_2 was identified as 4 equivalents (Ce: 2600 μg mL^{-1}). After confirming the optimal reaction of COS-CeO_2, the effect of loading time (2, 4, 6, 8 and 10 h) on loading efficiency and SP integrity was further evaluated. When reacted for 4 h, high loading efficiency and intact SP morphology were simultaneously achieved. Therefore, the loading time of 4 h was selected as the optimal time for SP@COS-CeO_2 synthesis
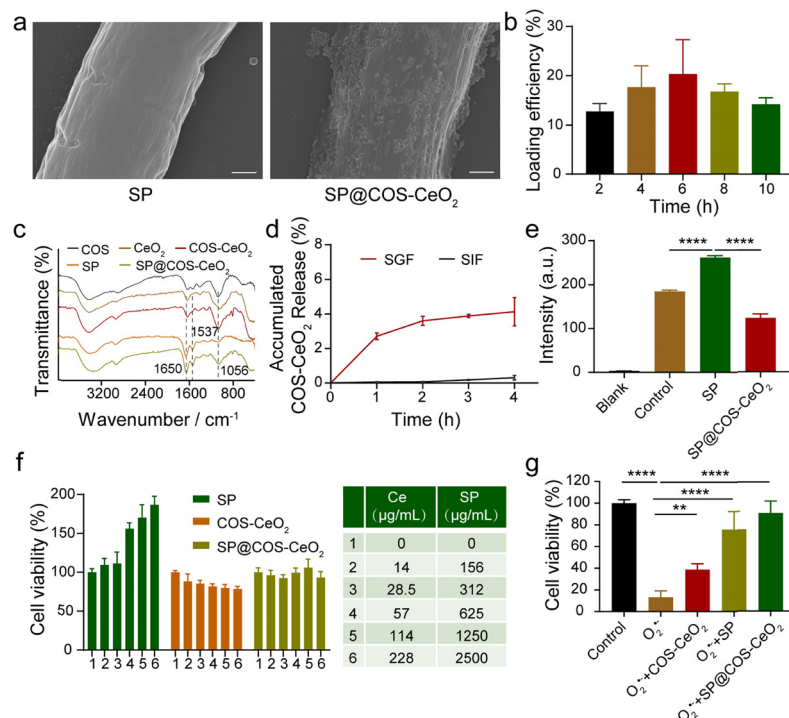
Fig. 2 Synthesis and characterization of SP@COS-CeO$_2$. (a) SEM images of SP and SP@COS-CeO$_2$. Scale bar = 1 μm. (b) The loading efficiency of COS-CeO$_2$ in SP (500 μg mL^{-1}) after reacting for 2, 4, 6, 8 and 10 h, respectively. (c) Fourier transform infrared (FTIR) spectra of the indicated materials. (d) Release profiles of COS-CeO$_2$ from SP@COS-CeO$_2$ in SIF (pH = 6.8; trypsin: 10 mg mL^{-1}) and SGF for 4 h. (e) Evaluation of cascade catalysis by detecting H$_2$O$_2$ accumulation using a H$_2$O$_2$-specific fluorescent probe (ROSGreen^{TM} H$_2$O$_2$ Probe). Data are presented as mean ± SD; n = 3. The statistical significance was calculated via one-way ANOVA with Tukey's multiple comparisons test. ****P < 0.0001. (f) Cell viability of NCM460 cells after incubating with different concentrations of SP, COS-CeO$_2$, and SP@COS-CeO$_2$ for 24 h. (g) Cytoprotection ability of SP, COS-CeO$_2$, and SP@COS-CeO$_2$ after co-incubation with O$_2$$^{•-}$ initiator of pyrogallol. Data are presented as mean ± SD; n = 5. The statistical significance was calculated via one-way ANOVA with Tukey's multiple comparisons test. **P < 0.01, ****P < 0.0001.

(Fig. 2b and Fig. S6, ESI†). The stability of the synthesized SP@COS-CeO$_2$ was tested by co-incubating with SGF and simulated intestinal fluid (SIF). It was found that less than 4% of the loaded COS-CeO$_2$ fell out of the SP surface after co-incubation with both SGF and SIF (Fig. 2d), demonstrating the potential stability of SP@COS-CeO$_2$ in the gastrointestinal tract.

To illustrate that SP@COS-CeO$_2$ can execute a cascade reaction to eliminate O$_2$$^{•-}$, pyrogallol (O$_2$$^{•-}$ initiator) and H$_2$O$_2$-specific fluorescent probe (ROSGreen^{TM} H$_2$O$_2$ Probe) were added to solutions containing SP or SP@COS-CeO$_2$. Under alkaline conditions, pyrogallol undergoes autooxidation accompanied by the production of O$_2$$^{•-}$, which will be converted to H$_2$O$_2$ under the mediation of SP owing to the catalysis of the intrinsic SOD. The steady fluorescence enhancement of H$_2$O$_2$-specific fluorescent probe proved the production of H$_2$O$_2$ when co-incubated with SP. While the fluorescence intensity of the solution containing SP@COS-CeO$_2$ was dramatically reduced by about 50% (Fig. 2e), which was ascribed to the decomposition of the H$_2$O$_2$ produced by loaded CeO$_2$ on SP, demonstrating that SP@COS-CeO$_2$ can effectively transform O$_2$$^{•-}$ to ultimate water and oxygen through a cascade reaction for O$_2$$^{•-}$ and H$_2$O$_2$ elimination.

To further evaluate the potential biomedical applicability of SP@COS-CeO$_2$ in the gastrointestinal tract, we first examined the cell toxicity of SP, COS-CeO$_2$, and SP@COS-CeO$_2$ on

NCM460 cells by a methyl thiazolyl tetrazolium (MTT) assay. Notably, SP had a significant growth promotion effect on NCM460 cells, while COS-CeO$_2$ showed negligible cytotoxicity. Combining the cell cytotoxicity effect of SP and COS-CeO$_2$, SP@COS-CeO$_2$ showed neither cytotoxicity nor cell growth promotion (Fig. 2f). As many living microalgae and nanomaterials could reduce MTT,[31,32] the growth promotion of SP toward NCM460 cells could be attributed to MTT reduction by live SP. Additionally, COS-CeO$_2$ has no effect on MTT reduction, as demonstrated in Fig. 2f, and the stable attachment of COS-CeO$_2$ onto the SP surface could shield the reduction effect of SP; therefore, SP@COS-CeO$_2$ exhibited neither cytotoxicity nor cell growth promotion. Overall, the final SP@COS-CeO$_2$ biohybrid is nontoxic to normal cells. Subsequently, we further investigated the ability of SP@COS-CeO$_2$ to eliminate O$_2$$^{•-}$ to protect cells. Pyrogallol and SP, COS-CeO$_2$ or SP@COS-CeO$_2$ were added to the medium and incubated with NCM460 cells for 24 h, respectively, and then the survival rate of the cells was detected by MTT assay. As shown in Fig. 2g, the cells treated with pyrogallol alone had a high mortality rate of more than 80% owing to production of cytotoxic O$_2$$^{•-}$, while the cells treated with SP@COS-CeO$_2$ had a significantly higher survival rate compared to COS-CeO$_2$ and SP, proving that SP@COS-CeO$_2$ had an excellent protective effect on the cells.

2.4. Anti-inflammation therapy for UC

As discussed above, SP@COS-CeO$_2$ can effectively eliminate the ROS O$_2^{\bullet-}$ and H$_2$O$_2$ through a tandem catalytic reaction. Next, we investigated the anti-inflammatory capacity of this strategy based on the combined catalysis of microalgal bioenzyme and artificial nanozyme in the treatment of IBD. IBD is a chronic, nonspecific inflammatory disease that includes UC and CD. We first evaluated the therapeutic effect of SP@COS-CeO$_2$ on

dextran sulfate sodium (DSS)-induced UC in C57BL/6 mice. 8-Week old mice were randomly divided into groups of control, DSS, COS-CeO$_2$, SP and SP@COS-CeO$_2$ ($n = 5$). After one week of acclimation, the drinking water of the mice was changed into 3% DSS for 6 days to trigger the occurrence of UC. In the treatment groups, COS-CeO$_2$, SP or SP@COS-CeO$_2$ were administered by gavage on days 4, 6, 8, 10 and 12 (Fig. 3a). After DSS induction, the bodyweight of the mice was recorded once every
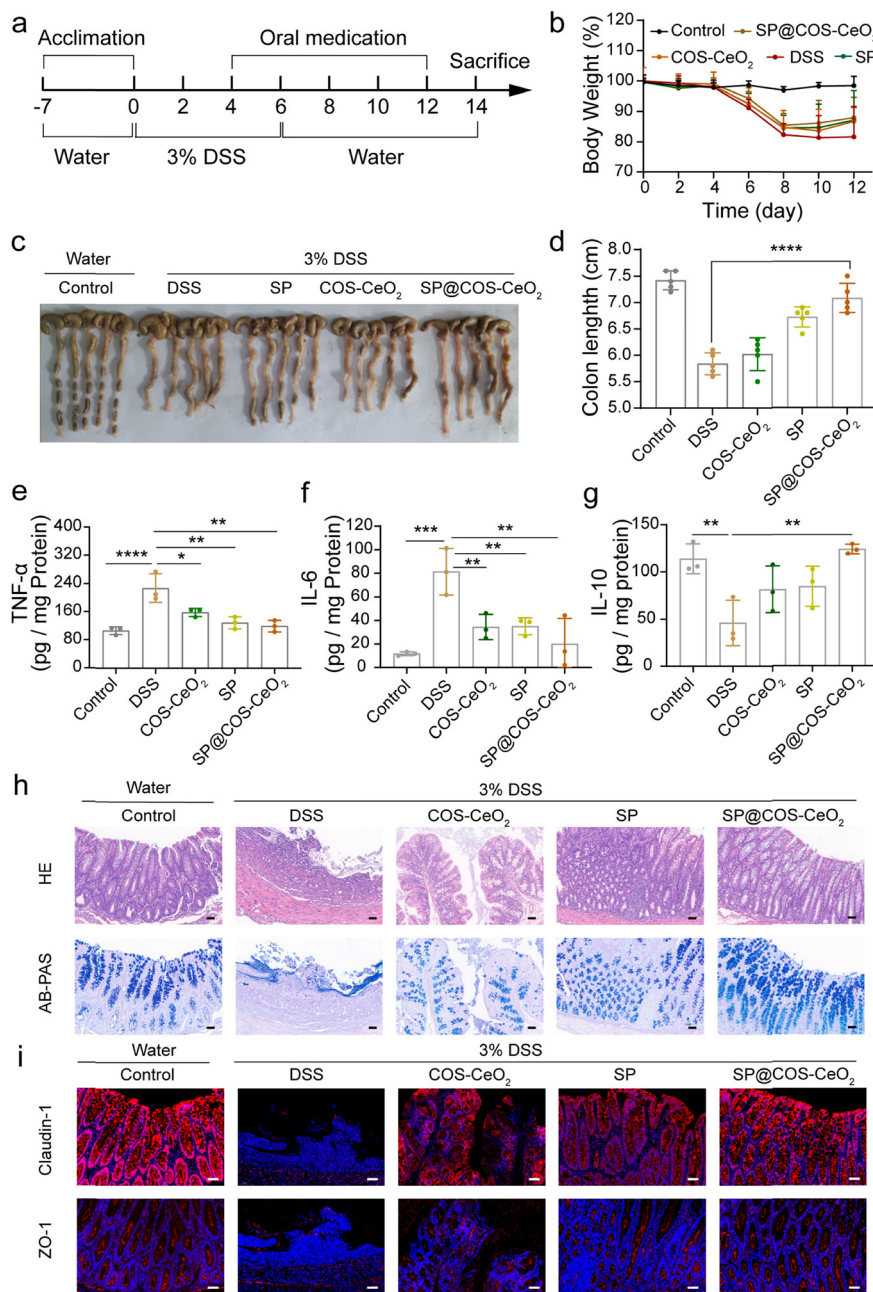

Fig. 3 Treatment efficacy of SP@COS-CeO$_2$ on against DSS-induced UC. (a) Overall procedure for the treatment of DSS-induced UC. (b) The bodyweight development of the mice in different groups. (c) Picture of the excised colon and (d) corresponding colon length. Data are presented as mean ± SD; $n = 5$. The statistical significance was calculated *via* one-way ANOVA with Tukey's multiple comparisons test. ****$P < 0.0001$. (e–g) The levels of TNF-α, IL-6 and IL-10 in colon homogenates. Data are presented as mean ± SD; $n = 3$. The statistical significance was calculated *via* one-way ANOVA with Tukey's multiple comparisons test. *$P < 0.05$, **$P < 0.01$, ***$P < 0.001$, ****$P < 0.0001$. (h) Representative images of H&E staining and AB-PAS staining. (i) Immunofluorescence staining of colonic claudin-1 and ZO-1 in different treatments. Scale bar: 50 μm.

two days. The experimental results revealed that only DSS treatment caused significant bodyweight loss compared to the control group, while the treatment groups restored the bodyweight loss to some extent, especially co-treating with

SP@COS-CeO$_2$ (Fig. 3b). After the mice were sacrificed, the colon was excised and the colon length was measured. As shown in Fig. 3c and d, the average colon length in the DSS group (5.8 ± 0.2 cm) was significantly shortened in comparison
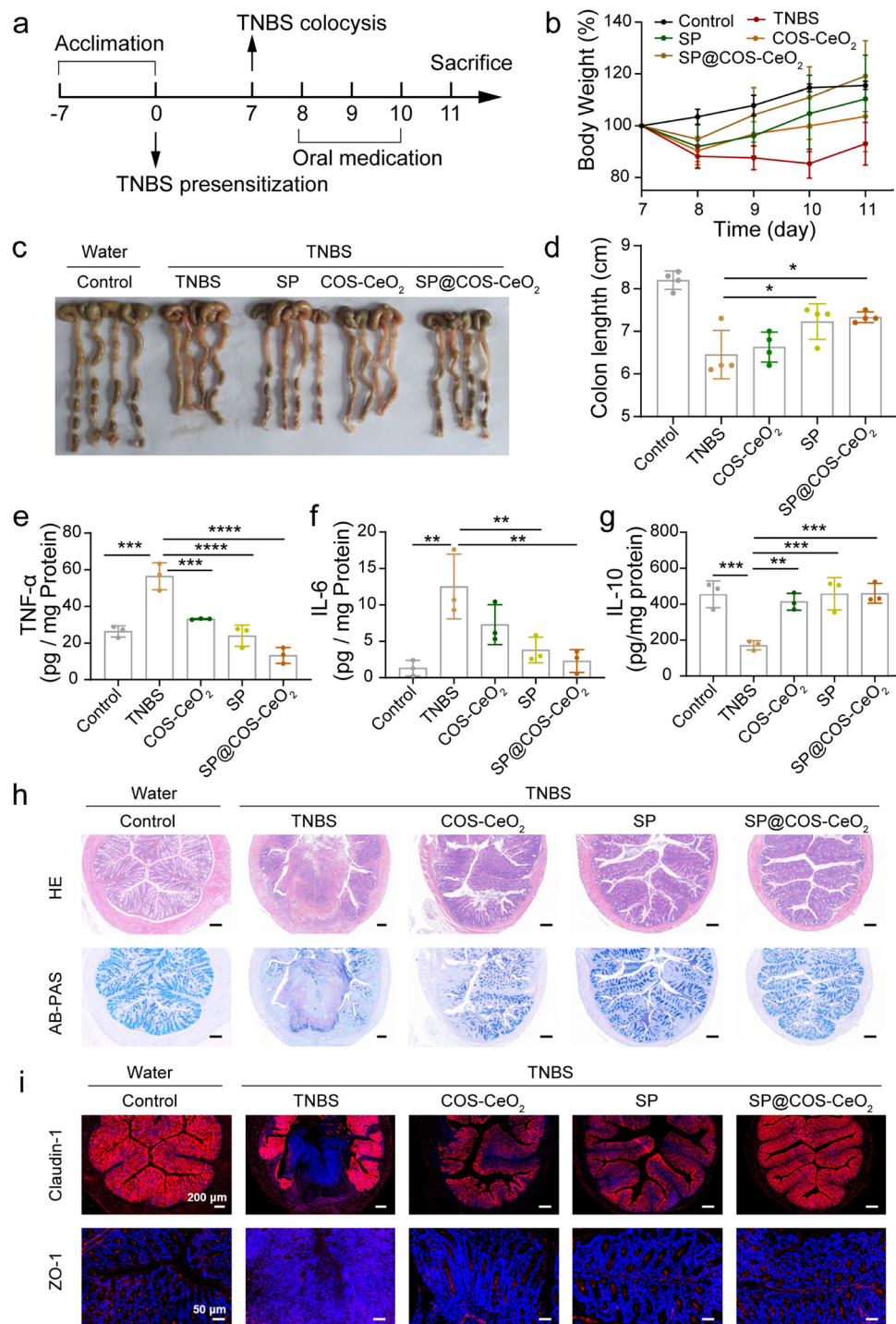

Fig. 4 Treatment efficacy of SP@COS-CeO$_2$ against TNBS-induced CD. (a) Overall procedure for the treatment of CD. (b) The bodyweight development of mice in different treatment groups. (c) Images of the colons and (d) corresponding colon length. Data are presented as mean $\pm$ SD; $n = 4$. The statistical significance was calculated *via* one-way ANOVA with Tukey's multiple comparisons test. *$P < 0.05$. (e–g) The levels of TNF-α, IL-6 and IL-10 in colon homogenates. Data are presented as mean $\pm$ SD; $n = 3$. The statistical significance was calculated *via* one-way ANOVA with Tukey's multiple comparisons test. **$P < 0.01$, ***$P < 0.001$, ****$P < 0.0001$. (h) Representative images of H&E staining and AB-PAS staining (scale bar: 200 µm). (i) Immunofluorescence staining images of colonic claudin-1 and ZO-1 in different treatments.

to the control group (7.4 $\pm$ 0.2 cm), indicating significant colonic inflammatory lesions in DSS treatment. However, the colon length in the COS-CeO$_2$, SP and SP@COS-CeO$_2$ groups had recovered to 6.02 $\pm$ 0.3 cm, 6.72 $\pm$ 0.2 cm and 7.1 $\pm$ 0.3 cm, respectively, indicating that treatment with these materials could alleviate the symptoms of DSS-induced colitis. Notably, the SP@COS-CeO$_2$ group has the most prominent colon protection effect.

To further evaluate the treatment effect of SP@COS-CeO$_2$ on UC, inflammation-related cytokines in colon tissues were detected. As shown in Fig. 3e–g, compared with the control group, the expressions of pro-inflammatory factors of tumor necrosis factor-α (TNF-α) and interleukin-6 (IL-6) were significantly elevated after DSS treatment. In the groups with COS-CeO$_2$, SP and SP@COS-CeO$_2$ intervention, SP@COS-CeO$_2$ exhibited the most significant inhibition effect on the expressions of TNF-α and IL-6. In contrast, the level of the anti-inflammatory factor of interleukin-10 (IL-10) were obviously lowered in DSS treatment, which was prominently increased after SP@COS-CeO$_2$ gavage, to become nearly identical to the expression of the control group. These data proved the superior anti-inflammation effect of SP@COS-CeO$_2$ on UC. Furthermore, we evaluated the histopathological changes in the colon. As shown by hematoxylin & eosin (H&E) staining (Fig. 3h), the colonic tissue of the DSS group displayed obvious diffuse infiltration of inflammatory cells, disappearance of the epithelial structure, mucosal erosion, edema, and crypt atrophy. In the co-treatment groups, COS-CeO$_2$ and SP treatment slightly improved the above inflammation and tissue damage in mice, while SP@COS-CeO$_2$ treatment displayed a significant protection effect on colon tissue with the restoration of epithelial structure, a close arrangement of crypts and reduction of inflammatory cells. Loss of goblet cells is one of the main characteristics of colitis, which also indicates the decreased secretion of mucopolysaccharides. Observing the changes in the number of goblet cells and mucopolysaccharide content is an important morphological basis for the diagnosis of changes in intestinal structure and function. According to Alcian blue & periodic acid Schiff (AB-PAS) staining (Fig. 3h), the goblet cells in the control group were densely arranged on both sides of the crypt, and the shape was regular and full. In the DSS group, the epithelial structure was destroyed, crypts disappeared, and goblet cells and mucus significantly decreased. After co-treatment with COS-CeO$_2$ and SP, the number of goblet cells and mucin expression slightly improved, while the most dramatic recovery was observed in the SP@COS-CeO$_2$ group, which had almost recovered to the level of the control group. Then, the integrity of the colonic epithelial mucosa and intestinal barrier function were evaluated by immunofluorescence staining of ZO-1 and claudin-1, which are the major tight junction associated proteins of the intestinal mucosa, playing a crucial role in maintaining the structure and function of intestinal epithelial cells and the integrity of the intestinal barrier. As shown in Fig. 3i, the expression of ZO-1 and claudin-1 was severely disrupted in the DSS group. Compared with COS-CeO$_2$ and SP treatment, SP@COS-CeO$_2$ treatment more effectively preserved the expression of ZO-1 and claudin-1. These data demonstrated the satisfactory therapeutic effect of SP@COS-CeO$_2$ against DSS-induced UC.

2.5. Anti-inflammation therapy for CD

To explore the breadth of therapeutic application of SP@COS-CeO$_2$ on inflammatory disease, we further evaluated the therapeutic efficacy of SP@COS-CeO$_2$ on CD. 2,4,6-Trinitrobenzenesulfonic acid (TNBS) was used to induce CD and the overall experimental procedure is shown in Fig. 4a. The successful onset of CD on day 8 was indicated by bodyweight loss in the mice. Oral gavage of COS-CeO$_2$, SP, or SP@COS-CeO$_2$ to TNBS-treated mice for three consecutive days (day 8 to day 10) was used to investigate the therapeutic efficiency. In contrast to COS-CeO$_2$ and SP, SP@COS-CeO$_2$ exhibited superior protection effect against TNBS-induced bodyweight loss (Fig. 4b) and colon shortening in the mice (Fig. 4c and d). In addition, TNBS promoted the expression of pro-inflammatory TNF-α and IL-6, and inhibited the anti-inflammatory factor of IL-10 in mice. We observed that SP@COS-CeO$_2$ treatment was more effective in restoring these cytokines to a normal level than COS-CeO$_2$ or SP treatment (Fig. 4e–g). According to histological analysis of H&E staining and AB-PAS staining (Fig. 4h), major signs of CD, such as ulceration, inflammatory cell infiltration, crypt deformation, and reduction in goblet cells and mucin, were clearly manifested in the colonic sections of only-TNBS-challenged mice. After co-treatment with COS-CeO$_2$ and SP, the above signs were relieved to some extent, while they dramatically improved after treatment with SP@COS-CeO$_2$. Besides, the immunofluorescence staining of ZO-1 and claudin-1 further confirmed that SP@COS-CeO$_2$ significantly restored the intestinal epithelial barrier (Fig. 4i). These characterizations clearly demonstrated that SP@COS-CeO$_2$ effectively ameliorated the symptoms of CD.

3. Conclusions

In summary, a biotic/abiotic biohybrid system that combines a microalgal bioenzyme with an inorganic nanoenzyme was developed. The biohybrid integrates the catalytic activity of the two components to execute a cascade reaction to eliminate the ROS O$_2^{\bullet-}$ and H$_2$O$_2$. *In vitro* and *in vivo* studies showed that the biohybrid system had excellent ROS scavenging activity, and showed excellent anti-inflammation ability in IBD of both UC and CD mouse models. This study proposes the combined application of biotic/abiotic biomaterials in biomedicine by integrating their catalytic activity.

4. Experimental section

4.1. Materials

S. platensis (SP) was purchased from Guangyu Biological Technology, Shanghai, China. Zarrouk medium was obtained from the Institute of Hydrobiology, Chinese Academy of Sciences. Cerium nitrate hexahydrate (Ce(NO$_3$)$_3$·6H$_2$O) was purchased from Shanghai Lingfeng Chemical Reagent Co., Ltd. 6-Aminohexanoic

acid (AHA), ammonia solution (NH_3, 25–28%), hydrogen per-oxide (H_2O_2, 30%) and chito-oligosaccharide (COS) were purchased from Sinopharm Chemical Reagent Co., Ltd. A Total Superoxide Dismutase Assay kit with WST-8 was purchased from Beyotime Biotechnology Co., Ltd. Pyrogallol was obtained from Heowns Biochem Technologies, LLC, Tianjin. Dextran sulfate sodium (DSS) was purchased from Meilunbio. 2,4,6-Trinitrobenzenesulfonic acid (TNBS) was purchased from Sigma-Aldrich.

4.2. Culture and collection of *S. platensis*

SP was cultured in Zarrouk medium containing 13.61 g L^{-1} $NaHCO_3$, 4.03 g L^{-1} Na_2CO_3, 0.5 g L^{-1} K_2HPO_4, 2.5 g L^{-1} $NaNO_3$, 1 g L^{-1} K_2SO_4, 1 g L^{-1} NaCl, 0.2 g L^{-1} $MgSO_4\cdot7H_2O$, 0.04 g L^{-1} $CaCl_2\cdot2H_2O$, 0.01 g L^{-1} $FeSO_4\cdot7H_2O$ and 1 mL L^{-1} trace metal solution in an incubator with a photoperiod of 12 h light/12 h dark and an intensity of 2000 lux. SP was collected with a pressing cloth with a diameter of 5 μm, then thoroughly cleaned with deionized water, and freeze-dried for further use.

4.3. Synthesis of CeO_2 and COS-CeO_2

Firstly, $Ce(NO_3)_3\cdot6H_2O$ (0.25 mmol) was dissolved in deionized water (10 mL), and ammonia solution (1 mL, 33%) was added drop by drop at room temperature. After stirring for 1 min, the mixture was heated to 95 °C. Meanwhile, AHA (1 mmol) and HCl (5 μL, 37%) were dissolved in deionized water (1 mL), and then injected into cerium nitrate solution with a syringe and reacted for 6 h under magnetic stirring. After reaction, the product was cooled to room temperature and sonicated for 15 min. The large particles were first separated by centrifugation (3000 rpm), the supernatant was collected and washed three times (10 000 rpm), and then dispersed in deionized water (5 mL). To obtain COS-CeO_2, the above CeO_2 suspension was added dropwise to 5 mL of COS solution (10 mg mL^{-1}) and stirred for 12 h at room temperature. The precipitate was collected by centrifugation (10 000 rpm) and washed with deionized water to remove excess COS, then dispersed into 5 mL of deionized water.

4.4. Synthesis of SP@COS-CeO_2

For the synthesis of SP@COS-CeO_2, lyophilized SP (5 mg) was dispersed into deionized water (10 mL) followed by dropwise addition of COS-CeO_2 suspension (1 mL). The mixture was stirred slowly at room temperature for 4 h, the precipitate was collected by centrifugation and washed three times, and finally stored in 1 mL of water.

4.5. SOD activity of SP

The SOD activity of SP was assessed using an SOD assay kit (Total Superoxide Dismutase Assay Kit with WST-8). First, lyophilized SP (5 mg) was treated with SOD sample preparation solution (200 μL) for 15 min (4 °C), and the supernatant was separated by centrifugation (12 000 g, 4 °C). Then, the super-natant (20 μL), pre-concentrated WST-8/enzyme working solution (160 μL) and reaction starting working solution (20 μL) were successively placed in a 96-well plate, thoroughly

mixed and incubated at 37 °C for 30 min. Finally, the absor-bance at 450 nm was measured with a microplate reader. The SOD activity of SP was evaluated by measuring the amount of color reduction to calculate the removal rate of superoxide. The accuracy was assessed by repeated analysis ($n = 5$).

4.6. CAT-like activity of CeO_2 and COS-CeO_2 nanoparticles

The CAT-like activities of CeO_2 and COS-CeO_2 were evaluated by measuring the amount of oxygen produced by the decomposi-tion of H_2O_2 with a dissolved oxygen meter. CeO_2 and COS-CeO_2 suspensions (0, 40, 80, 120, 160, 200 μL with Ce content of 2600 μg mL^{-1}) were added to deionized water to make a final volume of 4 mL. Then, H_2O_2 (1 mL, 30%) was added to the above suspension and sealed with liquid paraffin. The amount of dissolved oxygen within 15 min was detected with a dissolved oxygen meter.

4.7. Evaluation of cascade catalysis of SP@COS-CeO_2

Firstly, SP (1000 μg mL^{-1}) or SP@COS-CeO_2 (SP: 1000 μg mL^{-1}; Ce: 455 μg mL^{-1}) was added to Tris–HCl solution (pH = 8.2), followed by the addition of pyrogarcinol solution (0.9 mM) and mixing thoroughly. After mixing for 20 min, a ROSGreen™ H_2O_2 Probe (5 μM) was added and incubated for 15 min in the dark at room temperature. Finally, the fluorescence intensity was detected.

4.8. Stability investigation of SP@COS-CeO_2 in SGF and SIF

The SP@COS-CeO_2 suspension was centrifuged (3000 rpm) and the precipitate was redispersed in SGF or SIF. The samples were shaken for 1 h, 2 h, 3 h or 4 h in a shaker at 37 °C, and then the supernatant was collected by centrifugation. The content of Ce in the supernatant was detected by ICP-AES.

4.9. Cell culture

Human normal colon epithelial cell line NCM460 were obtained from the China Centre for Type Culture Collection. The cells were maintained in Dulbecco's modified Eagle's medium (DMEM, Invitrogen) supplemented with 10% fetal bovine serum (FBS) and 1% penicillin/streptomycin solution in a 5% CO_2 incubator at 37 °C. Low-passage cells (5th to 25th passage) were used for the experiments.

4.10. Cytotoxicity assay

To test the cytotoxicity of the materials, NCM460 cells were cultured in 24-well plates (1 × 10^5 per well) overnight and incubated with different concentrations of SP@COS-CeO_2 (156, 312, 625, 1250 and 2500 μg mL^{-1} SP, corresponding to 14, 28.5, 57, 114 and 228 μg mL^{-1} Ce) through a Transwell chamber for 24 h, and the same amounts of SP and COS-CeO_2 were incubated with cells from the other two groups. Cell viability was determined using a standard methyl thiazolyl tetrazolium (MTT) assay kit.

4.11. Cytoprotection ability after co-incubation with $O_2^{\bullet-}$ initiator of pyrogallol

To evaluate the protective effect of the material on cells, NCM460 cells were grown in 24-well plates (1×10^5 per well) for 24 h. Then, the cells were incubated with DMEM containing pyrogallol (0.9 mM), pyrogallol + SP (SP: 5000 μg mL^{-1}; pyrogallol: 0.9 mM), pyrogallol + COS-CeO$_2$ (Ce: 556 μg mL^{-1}; pyrogallol: 0.9 mM) or pyrogallol + SP@COS-CeO$_2$ (SP: 5000 μg mL^{-1}; Ce: 556 μg mL^{-1}; pyrogallol: 0.9 mM). Cells in the control group were incubated with DMEM alone. After 24 hours, the cell viability was detected with a standard methyl thiazolyl tetrazolium (MTT) assay kit.

4.12. DSS-induced ulcerative colitis model of C57BL/6J mice

All the animal experiments were performed in accordance with the laboratory animal guidelines established by the Animal Center Experiment/A3-Lab of Wuhan University. All animal experiments were approved by the Institutional Center of Wuhan University.

Female C57BL/6J (6–8 weeks) mice were randomly divided into five groups: control, DSS, SP, COS-CeO$_2$ and SP@COS-CeO$_2$. Except for the control group, the drinking water of the mice was replaced with 3% DSS aqueous for the first 6 days. On days 4, 6, 8, 10 and 12, the DSS-treated mice were gavaged with 200 μL of PBS in the DSS group and 200 μL of SP (5000 μg mL^{-1}), COS-CeO$_2$ (Ce: 455 μg mL^{-1}) or SP@COS-CeO$_2$ (SP: 5000 μg mL^{-1}; Ce: 455 μg mL^{-1}) in the SP, COS-CeO$_2$, and SP@COS-CeO$_2$ groups, respectively. The bodyweight of the mice was recorded every two days. On day 14, mice in all groups were sacrificed and their colons were collected for further histopathological experiments.

4.13. TNBS-induced Crohn's disease model of C57BL/6J mice

Female C57BL/6J (6–8 weeks) mice were randomly divided into five groups: control, TNBS, SP, COS-CeO$_2$ and SP@COS-CeO$_2$. On day 0, the mice were firstly shaved on the back and then sensitized by applying 150 μL of 1% TNBS solution to the skin. After a 24 h fast, on day 7, the mice were firstly anesthetized with isoflurane, and then 100 μL of 1% TNBS was slowly injected into the rectum using a syringe-connected hose. Mice in the control group were injected with the same amount of PBS. The TNBS-treated mice were given 200 μL of PBS, SP (5000 μg mL^{-1}), COS-CeO$_2$ (455 μg mL^{-1}) or SP@COS-CeO$_2$ (SP: 5000 μg mL^{-1}; Ce: 455 μg mL^{-1}) by oral gavage on days 8, 9 and 10, and their bodyweight was monitored daily. The mice were sacrificed on day 11 and colonic tissues were collected for determination of colonic length and further histopathological examination.

4.14. Statistical analysis

Statistical analysis was performed using GraphPad Prism 8.0 software and analysis of variance (ANOVA) followed by Tukey's multiple comparisons test were used to compare differences between different treatment groups. All values ($n \geq 3$) were represented as the mean $\pm$ standard deviation (SD). Differences were considered statistically significant at $*P < 0.05$, $**P < 0.01$, $***P < 0.001$, $****P < 0.0001$.

Author contributions

X. Z. Zhang and Q. W. Chen conceived and designed the project. Q. W. Chen and M. W. Cao performed the experiments. J. Y. Qiao and Q. R. Li offered technical support and insights. All the authors discussed and wrote the manuscript.

Conflicts of interest

The authors declare no conflict of interest.

Acknowledgements

References

1 L.-H. Fu, C. Qi, J. Lin and P. Huang, *Chem. Soc. Rev.*, 2018, **47**, 6454–6472.

2 Y. Huang, J. Ren and X. Qu, *Chem. Rev.*, 2019, **119**, 4357–4412.

3 J. Wu, Y. Yu, Y. Cheng, C. Cheng, Y. Zhang, B. Jiang, X. Zhao, L. Miao and H. Wei, *Angew. Chem., Int. Ed.*, 2021, **60**, 1227–1234.

4 X. Cai, L. Jiao, H. Yan, Y. Wu, W. Gu, D. Du, Y. Lin and C. Zhu, *Mater. Today*, 2021, **44**, 211–228.

5 R. Yan, J. Ren, J. Wen, Z. Cao, D. Wu, M. Qin, D. Xu, R. Castillo, F. Li, F. Wang, Z. Gan, C. Liu, P. Wei and Y. Lu, *Adv. Mater.*, 2022, **34**, 2105670.

6 Y. Huang, Z. Liu, C. Liu, E. Ju, Y. Zhang, J. Ren and X. Qu, *Angew. Chem., Int. Ed.*, 2016, **55**, 6646–6650.

7 J. Liang, S. Gao, J. Liu, M. Y. B. Zulkifli, J. Xu, J. Scott, V. Chen, J. Shi, A. Rawal and K. Liang, *Angew. Chem., Int. Ed.*, 2021, **60**, 5421–5428.

8 N. Singh, M. A. Savanur, S. Srivastava, P. D'Silva and G. Mugesh, *Angew. Chem., Int. Ed.*, 2017, **56**, 14267–14271.

9 T. Man, C. Xu, X.-Y. Liu, D. Li, C.-K. Tsung, H. Pei, Y. Wan and L. Li, *Nat. Commun.*, 2022, **13**, 305.

10 J. Zhou, M. Li, Q. Chen, X. Li, L. Chen, Z. Dong, W. Zhu, Y. Yang, Z. Liu and Q. Chen, *Nat. Commun.*, 2022, **13**, 3432.

11 W.-H. Chen, M. Vazquez-Gonzalez, A. Zoabi, R. Abu-Reziq and I. Willner, *Nat. Catal.*, 2018, **1**, 689–695.

12 P. Zhang, D. Sun, A. Cho, S. Weon, S. Lee, J. Lee, J. W. Han, D.-P. Kim and W. Choi, *Nat. Commun.*, 2019, **10**, 940.

13 J. Huang, Z. Liu, B. J. Bloomer, D. S. Clark, A. Mukhopadhyay, J. D. Keasling and J. F. Hartwig, *Nat. Chem.*, 2021, **13**, 1186–1191.

14 W. Liang, P. Wied, F. Carraro, C. J. Sumby, B. Nidetzky, C.-K. Tsung, P. Falcaro and C. J. Doonan, *Chem. Rev.*, 2021, **121**, 1077–1129.

15 S. Fedeli, J. Im, S. Gopalakrishnan, J. L. Elia, A. Gupta, D. Kim and V. M. Rotello, *Chem. Soc. Rev.*, 2021, **50**, 13467–13480.

16 R. Singh, M. Kumar, A. Mittal and P. K. Mehta, *3 Biotech*, 2016, **6**, 174.

17 Q.-W. Chen, J.-Y. Qiao, X.-H. Liu, C. Zhang and X.-Z. Zhang, *Chem. Soc. Rev.*, 2021, **50**, 12576–12615.

18 W.-H. Chen, Q.-W. Chen, Q. Chen, C. Cui, S. Duan, Y. Kang, Y. Liu, Y. Liu, W. Muhammad, S. Shao, C. Tang, J. Wang, L. Wang, M.-H. Xiong, L. Yin, K. Zhang, Z. Zhang, X. Zhen, J. Feng, C. Gao, Z. Gu, C. He, J. Ji, X. Jiang, W. Liu, Z. Liu, H. Peng, Y. Shen, L. Shi, X. Sun, H. Wang, J. Wang, H. Xiao, F.-J. Xu, Z. Zhong, X.-Z. Zhang and X. Chen, *Sci. China: Chem.*, 2022, **65**, 1010–1075.

19 Q.-W. Chen, J.-W. Wang, X.-N. Wang, J.-X. Fan, X.-H. Liu, B. Li, Z.-Y. Han, S.-X. Cheng and X.-Z. Zhang, *Angew. Chem., Int. Ed.*, 2020, **59**, 21562–21570.

20 L. Sun, D. Zhang, Y. Sun, S. Wang and J. Cai, *Adv. Funct. Mater.*, 2018, **28**, 1707231.

21 A. Terzopoulou, M. Palacios-Corella, C. Franco, S. Sevim, T. Dysli, F. Mushtaq, M. Romero-Angel, C. Marti-Gastaldo, D. Gong, J. Cai, X.-Z. Chen, M. Pumera, A. J. DeMello, B. J. Nelson, S. Pane and J. Puigmarti-Luis, *Adv. Funct. Mater.*, 2022, **32**, 2107421.

22 D. Zhang, D. Zhong, J. Ouyang, J. He, Y. Qi, W. Chen, X. Zhang, W. Tao and M. Zhou, *Nat. Commun.*, 2022, **13**, 1413.

23 J. E. Cohen, A. B. Goldstone, M. J. Paulsen, Y. Shudo, A. N. Steele, B. B. Edwards, J. B. Patel, J. W. MacArthur, Jr., M. S. Hopkins, C. E. Burnett, K. J. Jaatinen, A. D. Thakore, J. M. Farry, V. N. Truong, A. T. Bourdillon, L. M. Stapleton, A. Eskandari, A. S. Fairman, W. Hiesinger, T. V. Esipova, W. L. Patrick, K. Ji, J. A. Shizuru and Y. J. Woo, *Sci. Adv.*, 2017, **3**, e1603078.

24 D. Zhong, D. Zhang, W. Chen, J. He, C. Ren, X. Zhang, N. Kong, W. Tao and M. Zhou, *Sci. Adv.*, 2021, **7**, eabi9265.

25 D. Zhong, Z. Du and M. Zhou, *View*, 2021, **2**, 20200189.

26 A. Sannasimuthu, V. Kumaresan, M. Pasupuleti, B. A. Paray, M. K. Al-Sadoon and J. Arockiaraj, *Algal Res.*, 2018, **35**, 519–529.

27 M. M. S. Ismaiel, Y. M. El-Ayouty, P. C. Loewen and M. D. Piercey-Normore, *J. Appl. Phycol.*, 2014, **26**, 1649–1658.

28 K. Desai and S. Sivakami, *World J. Microbiol. Biotechnol.*, 2007, **23**, 1661–1666.

29 Y. Lin, C. Xu, J. Ren and X. Qu, *Angew. Chem., Int. Ed.*, 2012, **51**, 12579–12583.

30 T. Yu, B. Lim and Y. Xia, *Angew. Chem., Int. Ed.*, 2010, **49**, 4484–4487.

31 J. Li and L. Song, *Phycologia*, 2007, **46**, 593–599.

32 H. Wang, W. Jiang, L. Yuan, L. Wang and H. Chen, *ACS Appl. Mater. Interfaces*, 2013, **5**, 1800–1805.